Optics Communications 410 (2018) 936–940

Contents lists available at ScienceDirect

Optics Communications

journal homepage: www.elsevier.com/locate/optcom

Study of gain-coupled distributed feedback laser based on high order surface gain-coupled gratings

Feng Gao [a,b], Li Qin [a], Yongyi Chen [a,*], Peng Jia [a,*], Chao Chen [a], LiWen Cheng [c], Hong Chen [a,b], Lei Liang [a], Yugang Zeng [a], Xing Zhang [a], Hao Wu [a], Yongqiang Ning [a], Lijun Wang [a]

[a] State Key Laboratory of Luminescence and Application, Changchun Institute of Optics, Fine Mechanics and Physics, Chinese Academy of Sciences, Changchun 130033, China

[b] University of Chinese Academy of Sciences, Beijing 100049, China

[c] College of Physics Science and Technology, Yang Zhou University, Yang Zhou 225002, China

ARTICLE INFO

Keywords:
Gain-coupled distributed feedback lasers
Semiconductor lasers
Single-longitudinal mode

ABSTRACT

Single-longitudinal-mode, gain-coupled distributed feedback (DFB) lasers based on high order surface gain-coupled gratings are achieved. Periodic surface metal p-contacts with insulated grooves realize gain-coupled mechanism. To enhance gain contrast in the quantum wells without the introduction of effective index-coupled effect, groove length and depth were well designed. Our devices provided a single longitudinal mode with the maximum CW output power up to 48.8 mW/facet at 971.31 nm at 250 mA without facet coating, 3dB linewidth (<3.2 pm) and SMSR (>39 dB). Optical bistable characteristic was observed with a threshold current difference. Experimentally, devices with different cavity lengths were contrasted on power–current and spectrum characteristics. Due to easy fabrication technique and stable performance, it provides a method of fabricating practical gain-coupled distributed feedback lasers for commercial applications.

1. Introduction

Distributed feedback (DFB) semiconductor lasers with stable single-mode, narrow-linewidth, and high-accuracy-wavelength characteristic are indispensable in pumping sources [1], differential absorption lidar (DIAL) [2], material processing [3] and integrated optics [4]. Index-coupled DFB lasers with a uniform refractive index have an inherent problem of lasing two degenerated modes [5]. Introduction of phase shift gratings can effectively remove mode degeneration [6] but could suffer from spatial hole burning (SHB) [7,8] at high output power, reducing side-mode suppression ratio (SMSR) and quantum efficiency [9]. Moreover, phase shift DFB lasers are fabricated by high-cost and time-consuming complex nanoscale lithography. On the other hand, high-quality antireflection coating is also essential [10] because of random facet phases [11], which are hard to control and affect the single mode yield and reliability. Recently, DFB lasers based on reconstruction-equivalent-chirp (REC) technology are proposed to achieve low-cost lithography but still require second epitaxial regrowth or nanoscale fabrication process [12,13].

Gain-coupled DFB (GC-DFB) lasers based on periodic gain (or loss) are another solutions to achieve single longitudinal mode [5]. Implementation of gain-coupled mechanism can remove mode degeneration [14], and realize a high single mode yield [15], facet immunity [16] and the insensitivity to external feedback [17]. However, complex technology are still required like epitaxial regrowth technology or electron beam lithography [18], making no difference with index-coupled DFB lasers and preventing them from widespread practical applications.

In this paper, a regrowth-free GC-DFB laser based on high order surface gain-coupled gratings was proposed. Periodic surface metal p-contact with insulated grooves acting as 32rd order gain-coupled gratings fabricated merely by i-line lithography caused periodic injection current, leading to gain contrast in quantum wells and forming gain-coupled mechanism without the effective index-coupled effect. Stable and high single-longitudinal-mode operation with SMSR (>39 dB), 3dB linewidth (<3.2 pm) were achieved. The SMSR was better than that of other high-order surface index-coupled gratings [19]. Optical bistable characteristic was observed around threshold current, which have potential to be applied as an optical transistor, memory element and differential amplifier [20]. Only low-cost ordinary i-line lithography

* Corresponding authors.
E-mail addresses: chenyy@ciomp.ac.cn (Y. Chen), jiapeng@ciomp.ac.cn (P. Jia).

http://dx.doi.org/10.1016/j.optcom.2017.09.023
Received 24 June 2017; Accepted 7 September 2017
Available online 1 November 2017
0030-4018/

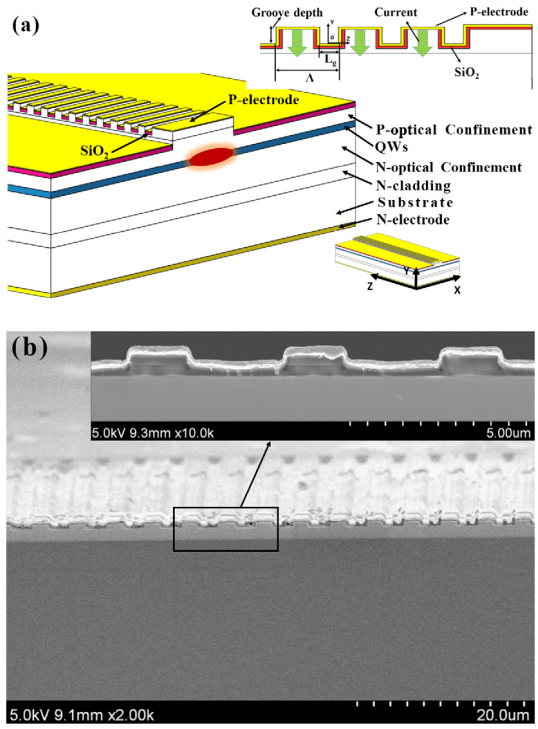

Fig. 1. (a) Device schematic (inset: periodic current injection operation schematic); (b) Scanning electron microscope image of cross section.

was used for pattern transfer without nanoscale lithography. Due to easy fabrication technique and stable performance, it provides a method to fabricate practical gain-coupled distributed feedback lasers for commercial applications.

2. Device structure design and fabrication

Fig. 1(a) shows the schematic of our device. Periodic p-contact and periodic grooves insulated by silica caused periodic injection current distribution, resulting a gain contrast in quantum wells to form gain-coupled mechanism. Silica with suitable thickness were filled in grooves, actually enhancing the insulativity of grooves, which was better than the oxidation of the bottom and side walls in grooves region with aluminum-doped layers in our previous research [21]. Considering the gain-coupled effect and index-coupled effect both introduced by surface grooves, the parameters of groove depth and length should be carefully designed to realize high gain contrast (large imaginary part of κ) and small index-coupled effect (small real part of κ).

κ represents the coupling coefficient [22]:

$$\kappa = \frac{k_0^2 \bar{n}_{eff}}{\beta_0} \frac{\int_{-\infty}^{+\infty} \Delta n_p(z)\, U^2(x,y)\, dz}{\int_{-\infty}^{+\infty} U^2(x,y)\, dz}, \tag{1}$$

where, $k_0 = \frac{2\pi}{\lambda_0}$ is the vacuum wave number for the vacuum wavelength λ_0. $\bar{n}_{eff}$ is the average mode effective index of the DFB structure. β_0 is propagation constant. $U(x,y)$ is the mode pattern. $\Delta\tilde{n}_p(z)$ is the Fourier factor of the p_{th} Fourier expansion for the mode effective index difference $\Delta\tilde{n}(z)$:

$$\Delta\tilde{n}(z) = \sum_{l=-\infty}^{\infty} \Delta\tilde{n}_p e^{i2\beta_B z}, \tag{2}$$

where, β_B represents the Bragg wave vector.

Noting that, when we consider the gain/loss and the refractive index change in the waveguide,

$$\Delta\tilde{n}(z) = \Delta n(z) + i\frac{\Delta g(z)}{2k_0}, \tag{3}$$

where, $\Delta g(z)$ represents the gain/loss change in the waveguide, and $\Delta n(z)$ is the refractive index change.

Consider a single period, and choose the center of the groove as original spot as shown in the inset in Fig. 1(a). Considering carrier vertical injection and side drift, we assume a cosine shape for the carrier density in the waveguide. As a linear relationship between model gain and carrier density [23], we have a cosine-shaped gain. Hence the rectangular form of index grating and cosine shape of gain are written as below:

$$\Delta n(z) = \Delta n = \begin{cases} n_{eff_0} - n_{eff_g} & \left(-\frac{L_g}{2} \le z \le \frac{L_g}{2}\right) \\ 0 & \left(-\frac{\Lambda}{2} \le z \le -\frac{L_g}{2}, \frac{L_g}{2} \le z \le \frac{\Lambda}{2}\right) \end{cases} \tag{4}$$

$$\Delta g(z) = \Delta g \cos\left(\frac{2l\pi}{\Lambda} z + \pi\right) \tag{5}$$

where, n_{eff_0} is the mode effective index of the waveguide, and n_{eff_g} is the mode effective index of the groove region in the grating. L_g represents the grating's groove length. Δn is the refractive index change in the waveguide. Λ is the period for the $l$order grating ($\Lambda = l\lambda/2\bar{n}_{eff}$).

As the Fourier transform based on Eq. (2),

$$\Delta\tilde{n}_p(z) = \frac{1}{\Lambda} \int_{-\frac{\Lambda}{2}}^{\frac{\Lambda}{2}} \Delta\tilde{n}(z)\, e^{i2\beta_B z} dz, \tag{6}$$

we have,

$$\Delta\tilde{n}_{+1}(z) = \Delta n \frac{\sin\left(\frac{l\pi}{\Lambda} L_g\right)}{l\pi} + i\frac{\Delta g}{4k_0}. \tag{7}$$

Considering $\bar{n}_{eff} \approx n_{eff_0} \approx n_{eff_g}$, the theoretical calculation for κ is

$$\kappa = k_0 \Gamma \left(\Delta n \frac{\sin\left(\frac{l\pi}{\Lambda} L_g\right)}{l\pi} + i\frac{\Delta g}{4k_0} \right) \tag{8}$$

where $\Gamma = 0.01185$ is the optical confinement factor in our device calculated by the commercial software COMSOL Multiphysics.

To realize small real part of κ, small Δn, large Λ and suitable L_g were desired based on Eq. (8). Hence, Λ was chosen to be 4.5 μm, much larger than nanoscale Bragg grating [24]. The relationship between Δn and groove depth was calculated by the commercial software COMSOL Multiphysics. Hence, based on Eq. (8) at fixed Λ (4.5 μm) and L_g (3 μm), the real part of κ as a function of groove depth was achieved as shown in Fig. 2(a), indicating that deeper grooves will enhance the index-coupled effect. Considering scattering loss from high order gratings and absorption loss from top p-contact in surface-etched grooves, we used a 2D simulation to estimate the relationship of etching depth and total loss. The total loss for one period at fixed Λ (4.5 μm) and L_g (3 μm) at different wavelengths were calculated by the commercial software COMSOL Multiphysics as shown in Fig. 3, and the optical field distributions in 600 nm and 1200 nm groove depth for one period are shown in Fig. 4 as demonstration: the device with groove depth of 600 nm could suffer from only less than 0.0015 power loss while 0.1607 at the depth of 1200 nm. It can be seen in Figs. 2(a) and 3, larger etching depth will lead to more index-coupled effect and more optical loss. It is better to have groove depth less than 700 nm in our devices.

On the other hand, the large imaginary part of κ was also indispensable to realize gain-coupled mechanism. The commercial software PICS3D was used to simulate the carrier density distribution in quantum wells for two periods with different groove length and depth. And by the linear relationship between model gain and carrier density [23], the gain contrast in quantum could be easily achieved. The imaginary part of κ having a linear relationship with the groove depth at fixed Λ (4.5 μm), L_g (3 μm) was shown in Fig. 2(b). The dependencies of groove length versus carrier density at the fixed period (4.5 μm) and groove depth (600 nm) as shown in Fig. 5, indicating that the increasing of groove length

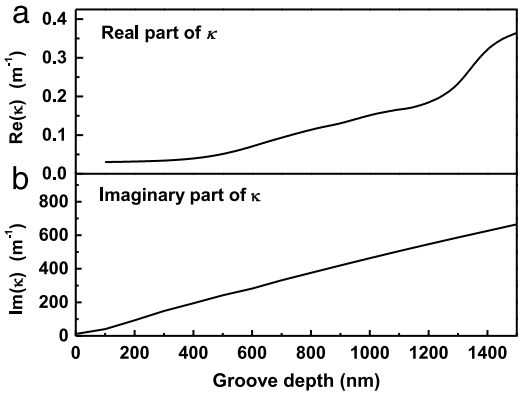

Fig. 2. The real part and imaginary part of calculated coupling coefficient κ as a function of groove depth with fixed period (4.5 μm) and groove length (3 μm).

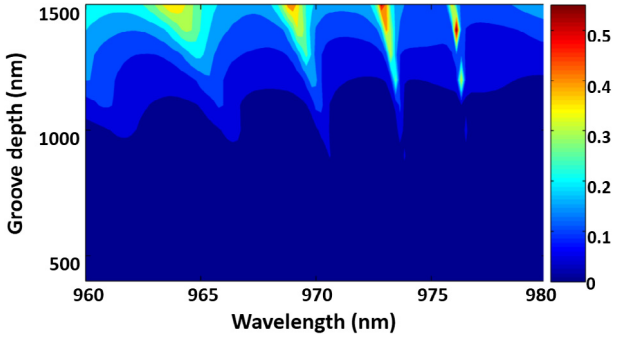

Fig. 3. The total loss from surface-etch groove for one period (4.5 μm) as a function of groove depth with fixed groove length (3 μm).

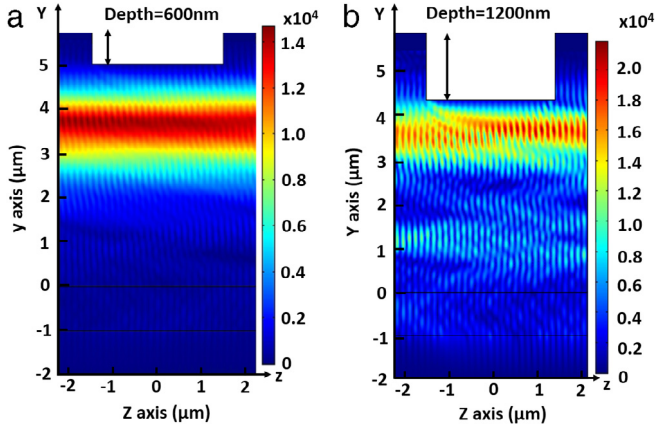

Fig. 4. The optical field distribution with fixed period (4.5 μm) and groove length (3 μm) (a) at 600 nm depth; (b) at 1200 nm depth.

can effectively reduce the side diffusion of injecting carrier and improve the contrast of carrier density in the quantum wells. So, considering the ordinary i-line lithography fabrication error (~1 μm), the designed groove length (on the photolithography mask) was chosen to 3 μm (1.5 μm for the length of residual region of one period). And, to realize small real part of κ, large imaginary part of κ within the fabrication tolerance range and small total loss, the groove depth was made trade off to be 550 ~ 700 nm.

The epitaxy for our devices grown by Metal Organic Chemical Vapor Deposition (MOCVD) was described in [21], including an asymmetric separate confinement heterostructure (SCH) with two AlGaInAs quantum wells lasing at around 970 nm. Formation of periodic grooves was

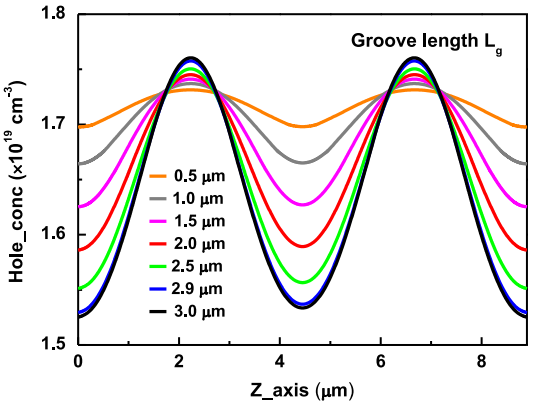

Fig. 5. 1D carrier density distribution in quantum wells for two periods at different groove length at fixed period (4.5 μm) and groove depth (600 nm).

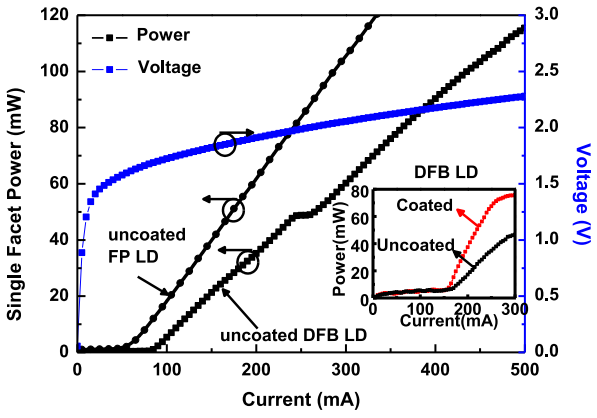

Fig. 6. Power–voltage–current characteristics in CW mode from FP and DFB lasers with 1 mm cavity length. (Inset: in contrast with the coated and uncoated device without packaged in pulse mode).

patterned only by i-line lithography and etched by Inductively Coupled Plasma (ICP). Because the fabrication error, the practical groove length was 2.9 μm and groove depth 570 nm, forming l = 32rd order Bragg grating, as shown in Fig. 1(b). Lateral waveguide was defined to 10 μm by i-line lithography and etched to 870 nm by ICP. Then, silica layer was deposited on the top of the epitaxy by plasma enhanced chemical vapor deposition (PECVD) and periodic current window structure was pattern by i-line lithography again. After metallization, the surface periodic metal p-contacts were formed with periodic grooves surrounded by silica. Finally, the chip was cleaved. The devices were packaged p-side down on C-mount heat sinks with water-cooling to maintain stationary temperature (20 °C). The spectrum was measured directly by coupling the laser using a 10 μm core diameter fiber-linking YOKOGAWA AQ6370C optical spectrum analyzer. The linewidth was measured by coupling collimating laser to Fabry–Perot Interferometer (Thorlabs, SA200-8B) with the oscilloscope.

3. Experiment results and discussion

CW power–voltage–current and spectrum characteristics from Fabry–Perot (FP) and DFB lasers with the 1 mm cavity length are shown in Figs. 6 and 7. The maximum CW power of uncoated DFB lasers at single longitudinal mode operation was up to 48.8 mW/facet at 250 mA. The slope efficiency in the uncoated GC-DFB lasers was 0.28 W/A, twice larger than 0.11 W/A of gain-coupled DFB lasers with a titanium surface Bragg grating [25], benefitting from removing plasma effect and loss from metal gratings. Compared with the uncoated FP laser only without

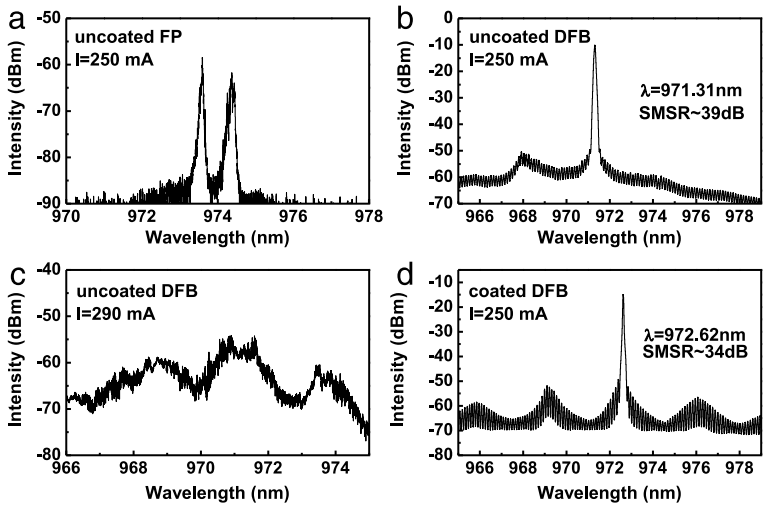

Fig. 7. CW spectrum characteristics for devices with 1 mm cavity length, (a) uncoated FP at 250 mA, (b) uncoated DFB at 250 mA (c) uncoated DFB at 290 mA, (d) coated DFB at 250 mA.

high order surface gain-coupled gratings, the slope efficiency dropped down. It was mainly because of periodic grooves actually coupled a small part of waveguide power acting as index-coupled gratings and the total loss was almost 0.12% for one period as shown in Fig. 3. In our practical devices, the calculated κ was only 0.0667 m^{-1} and κL0.0000667 for the cavity length of 1 mm. Compared with ordinary DFB lasers with κL more than 1 and for high order multiple longitudinal mode DFB lasers $\kappa L \sim 0.3$ [26], it caused a very weak index-coupled effect. And the carrier density distribution for two periods was shown in Fig. 8, indicating the obvious gain contrast in quantum wells. Hence, gain-coupled mechanism played an important role in mode selection.

The threshold current of the uncoated GC-DFB laser was 90.325 mA with the current increasing before lasing, which was greater than 90.051 mA when the current decreased and the laser was shutting off, causing a 0.274 mA threshold difference (measured by the OPHIR (Nova I) and Keithley 6200, a system error less than 1 μA). Optical bistable effect was observed around the threshold current. The physical mechanism was the nonlinear dependence of the absorption and gain coefficients in the saturable absorbing (insulated grooves region) and the gain region (current injection region) [27]. It could be determined that before lasing, photon density in our device was low while absorptivity was large in saturable absorption, causing grooves region at absorption state. So our device required a higher threshold gain to satisfy the lasing condition. After lasing, photon density is large and absorptivity is low, causing grooves region at transparent state. Devices with optical bistable characteristic could be applied in memory elements and optical switches, avoiding large sizes or complex fabrication step [28,29].

The actual lasing wavelength was 971.31 nm at 250 mA with side mode suppression radio (SMSR) over 39 dB while FP lasers operated at multi-longitudinal mode as shown in Fig. 7. The measured 3dB linewidth was only 3.2 pm, much better than the reported DFB laser with the linewidth of 10 pm [30]. There was a kinking in P-I-V characteristics as shown in Fig. 6. It was because of a clear transition from single-longitudinal mode to multiple-longitudinal mode operation, as experimentally shown in Fig. 7(b) and (c). After deposited on the facets by high reflectivity films (about 95% reflectivity) and anti-reflectivity films (about 5% reflectivity), the power of the same chip in pulsed mode could can be improved nearly 1.6 times as shown in the inset of Fig. 6. And the device was still operating at single longitudinal mode, as shown in Fig. 7(d).

Fig. 9 shows measured far-field patterns in CW mode. The beam divergence in slow axis at full width at half maximum (FWHM) was less than 6°, maintaining nearly Gaussian distribution with injection current increasing. The beam divergence in fast axis at FWHM was only

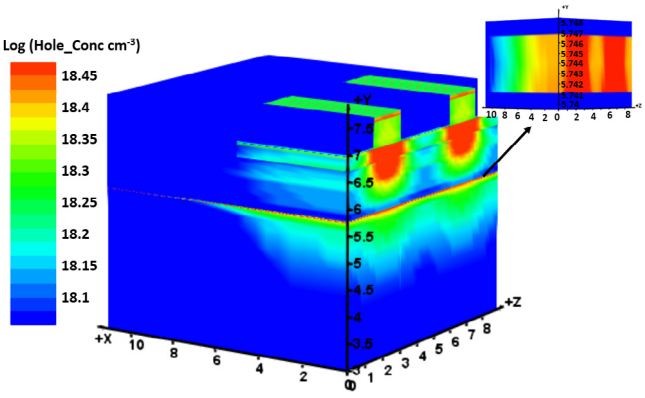

Fig. 8. Three-dimensional carrier density distribution for two periods, in a log scale with 4.5 μm period (2.9 μm groove length) and 570 nm groove depth. The inset shows 3D carrier density distribution in the quantum well.

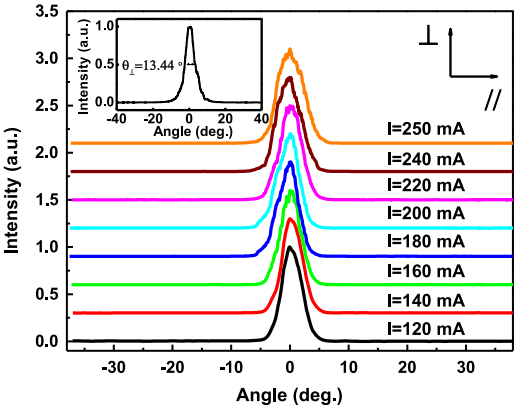

Fig. 9. Measured far-field pattern in the CW mode.

13. 44°, due to the design of asymmetric large optical cavity structure. Our device with a good beam quality were highly desirable for fiber coupling.

Fig. 10 shows the spectrum (I=200 mA) and power–current (inset) characteristics with different cavity length (0.6 mm/1 mm/1.6 mm) at fixed period (4.5 μm) and groove length (2.9 μm) groove depth (570

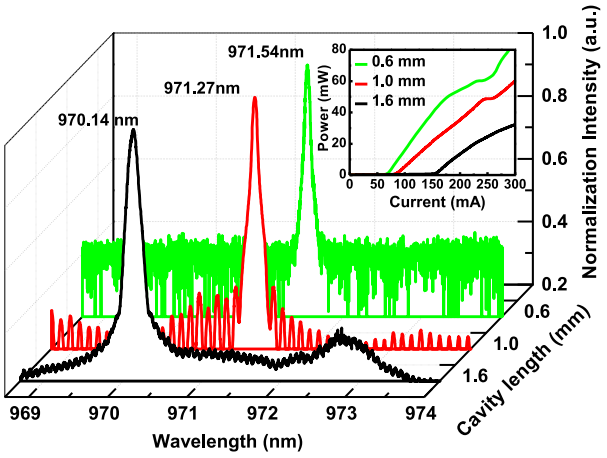

Fig. 10. Contrast of spectrum (I = 200 mA) and power–current (inset) characteristics as a function of cavity length (0.6 mm/1 mm/1.6 mm) at fixed period (4.5 μm) and groove length (2.9 μm) groove depth (570 nm).

nm), fabricated simultaneously on the same chip with same period (4.5 μm). Cavity length related to modal gain depending on injection current density [31], which caused the threshold current of device with longer cavity length increased. Considering the injection current density at the same current injection, devices with shorter cavity length had the larger current density, causing higher heat accumulation and wavelength "red" shift.

4. Conclusion

A single-longitudinal-mode regrowth-free gain-coupled DFB laser based on high order surface gain-coupled gratings was demonstrated, fabricated by only low-cost i-line lithography without regrowth and nanoscale lithography. By optimized groove length and depth, our devices realized a large gain contrast in quantum well without the effective index-coupled effect. Our uncoated devices with 1 mm cavity length could provide stable single longitudinal mode operation with the maximum CW output power up to 48.8 mW/facet at 971.31 nm at 250 mA, linewidth (<3.2 pm) and SMSR (>39 dB). And the SMSR is better than that of other high-order surface index-coupled gratings [19]. Compared with the existing gain-coupled DFB lasers with a titanium surface Bragg grating [25], our devices remove the most of loss from metal gratings, improving the slope efficiency (0.28 W/A, twice larger than 0.11 W/A [25]). Optical bistable characteristic was observed around threshold current with a 0.274 mA threshold current difference, which have potential for widespread applications as an optical transistor, memory element and differential amplifier. Experimentally, devices with different cavity length were contrasted on power–current and spectrum characteristics. Due to easy fabrication technique and stable performance, it provides a method to fabricate practical gain-coupled distributed feedback lasers for widespread commercial applications. Future work will concentrate on the applications such as single-chip multiple-wavelength sources.

Acknowledgments

This work was supported by National Natural Science Foundation of China (NSFC) (61234004, 51672264, 61674148, 11604328, 11404327, 61235004, 61404114, 61505206); National Science and Technology Major Project of China (2016YFE0126800); Frontier Science Key Program of the President of the Chinese Academy of Sciences (QYZDY-SSW-JSC006); Natural Science Foundation of Jilin Province (Jilin Province Natural Science Foundation) (20150203007GX, 20150204042GX, 20160414016GH).

References

[1] R. Paschotta, J. Nilsson, A.C. Tropper, D.C. Hanna, Ytterbium-doped fiber amplifiers, IEEE J. Quantum Electron. 33 (1997) 1049–1056.
[2] A.R. Nehrir, K.S. Repasky, J.L. Carlsten, Eye-safe diode-laser-based micropulse differential absorption lidar (DIAL) for water vapor profiling in the lower troposphere, J. Atmos. Ocean. Technol. 28 (2011) 131–147.
[3] W. Schulz, R. Poprawe, Manufacturing with novel high-power diode lasers, IEEE J. Sel. Top. Quantum Electron 6 (2000) 696–705.
[4] Z. Zhou, B. Yin, J. Michel, On-chip light sources for silicon photonics, Light Sci. Appl. 4 (2015) e358.
[5] H. Kogelnik, C.V. Shank, Coupled-wave theory of distributed feedback lasers, J. Appl. Phys. 43 (1972) 2327–2335.
[6] S. Nilsson, T. Kjellberg, T. Klinga, R. Schatz, J. Wallin, K. Streubel, Improved spectral characteristics of MQW-DFB lasers by incorporation of multiple phase-shifts, J. Lightwave Technol. 13 (1995) 434–441.
[7] H. Soda, H. Ishikawa, H. Imai, Design of DFB lasers for high-power single-mode operation, Electron. Lett 22 (1986) 1047–1049.
[8] L.J.P. Ketelsen, I. Hoshino, D.A. Ackerman, Experimental and theoretical evaluation of the CW suppression of TE side modes in conventional 1.55 μm InP-InGaAsP distributed feedback lasers, IEEE J. Quantum Electron. 27 (1991) 965–975.
[9] H. Soda, Y. Kotaki, H. Sudo, H. Ishikawa, Stability in single longitudinal mode operation in GaInAsP/InP phase-adjusted DFB lasers, IEEE J. Quantum Electron. 23 (1987) 804–814.
[10] S.R. Chinn, Effects of mirror reflectivity in a distributed-feedback laser, IEEE J. Quantum Electron. 9 (1973) 574–580.
[11] H. Haus, C.V. Shank, Antisymmetric taper of distributed feedback lasers, IEEE J. Quantum Electron. 12 (9) (1976) 532–539.
[12] R.J. Guo, J. Lu, S.P. Liu, Y.C. Shi, Y.T. Zhou, Y.T. Chen, J. Luan, X.F. Chen, Multisection DFB tunable laser based on REC technique and tuning by injection current, IEEE Photon. J. 8 (2016) 7.
[13] Y. Shi, S. Li, R. Guo, R. Liu, Y. Zhou, X. Chen, A novel concavely apodized DFB semiconductor laser using common holographic exposure, Opt. Express 21 (2013) 16022–16028.
[14] E. Kapon, A. Hardy, A. Katzir, The effect of complex coupling coefficients on distributed feedback lasers, IEEE J. Quantum Electron. 18 (1982) 66–71.
[15] S.T. Kim, B.G. Kim, Analysis of single-mode yields above threshold for complex-coupled distributed feedback lasers with asymmetric facet reflectivities, J. Opt. Soc. Am. B. 22 (2005) 1010–1015.
[16] N. Susa, Fluctuations of the laser characteristics and the effect of the index-coupling component in the gain-coupled DFB laser, IEEE J. Quantum Electron. 33 (1997) 2255–2265.
[17] A.J. Lowery, D. Novak, Performance comparison of gain-coupled and index-coupled DFB semiconductor lasers, IEEE J. Quantum Electron. 30 (1994) 2051–2063. IEEE Photonics Technology Letters.
[18] Y. Luo, Y. Nakano, K. Tada, T. Inoue, H. Hosomatsu, H. Iwaoka, Purely gain-coupled distributed feedback semiconductor laser, Appl. Phys. Lett. 56 (1990) 1620–1622.
[19] L. Liu, H. Qu, Y. Wang, Y. Liu, Y. Zhang, W. Zheng, High-brightness single-mode double-tapered laser diodes with laterally coupled high-order surface grating, Opt. Lett. 39 (2014) 3231–3234.
[20] H.G. Winful, J.H. Marburger, E. Garmire, Theory of bistability in nonlinear distributed feedback structures, Appl. Phys. Lett. 35 (1979) 379–381.
[21] Y. Chen, P. Jia, J. Zhang, L. Qin, H. Chen, F. Gao, X. Zhang, X. Shan, Y. Ning, L. Wang, Gain-coupled distributed feedback laser based on periodic surface anode canals, Appl. Opt. 54 (2015) 8863–8866.
[22] S.L. Chuang, Physics of Photonic Devices, Wiley, 2009.
[23] B.W. Hakki, Carrier and gain spatial profiles in GaAs stripe geometry lasers, J. Appl. Phys. 44 (1973) 5021–5028.
[24] A. Orth, J.P. Reithmaier, R. Zeh, H. Doleschel, A. Forchel, First order gain-coupled GaInAs/GaAs distributed feedback laser diodes patterned by focused ion beam implantation, Appl. Phys. Lett. 69 (1996) 1906–1908.
[25] T.W. Johannes, A. Rast, W. Harth, J. Rieger, Gain-coupled DFB lasers with a titanium surface Bragg grating, Electron. Lett 31 (1995) 370–371.
[26] J. Decker, P. Crump, J. Fricke, A. Maassdorf, G. Erbert, G. Trankle, Narrow stripe broad area lasers with high order distributed feedback surface gratings, IEEE Photon. Technol. Lett. 26 (2014) 829–832.
[27] S.I. Pegg, M.J. Adams, K. Poguntke, Simultaneous absorptive and dispersive all-optical switching of a multi-section bistable laser diode, Opt. Commun. 174 (2000) 191–194.
[28] Y.Z. Huang, S.J. Wang, Y.D. Yang, J.L. Xiao, Y.H. Hu, Y. Du, Optical bistability in InP/GaInAsP equilateral-triangle-resonator microlasers, Opt. Lett. 34 (2009) 1852–1854.
[29] S. Tan, M. Sun, D. Lu, R. Zhang, Bistable 1060-nm high power single mode DFB laser diode, IEEE Photon. J. 7 (2015) 1–1.
[30] T.N. Vu, A. Klehr, B. Sumpf, H. Wenzel, G. Erbert, G. Tränkle, Tunable 975 nm nanosecond diode-laser-based master-oscillator power-amplifier system with 16.3 W peak power and narrow spectral linewidth below 10 pm, Opt. Lett. 39 (2014) 5138–5141.
[31] C. Shieh, R. Engelmann, J. Mantz, K. Alavi, C. Shu, Cavity length dependence of threshold current for quantum well lasers, Appl. Phys. Lett. 54 (1989) 1089–1091.